

Available at www.sciencedirect.com

SciVerse ScienceDirect

journal homepage: www.elsevier.com/locate/carbon

An atomistic simulation study of the mechanisms and kinetics of surface bond strengthening in thermally-treated cone-stacked carbon nanofibers

Jingjun Gu ^a, Frederic Sansoz ^{a,b,*}

^a Mechanical Engineering Program, School of Engineering, The University of Vermont, Burlington, VT 05405, United States

^b Materials Science Program, The University of Vermont, Burlington, VT 05405, United States

ARTICLE INFO

Article history:

Received 20 October 2012

Accepted 12 January 2013

Available online 23 January 2013

ABSTRACT

Bonding mechanisms and rates between the active edges of a cone-stacked CNF are examined by molecular dynamics simulations at temperatures up to 2273 K. Thermally treated nanofibers subjected to tensile deformation show a substantial increase in the elastic strain limit, albeit no change in elastic modulus, due to the resistance of surface bonds to crack propagation. Two bonding mechanisms; i.e., the formation of energetically stable loops from single dangling atoms and the folding of zigzag and armchair graphene bilayer edges, are shown to display predominant, yet distinct kinetics. This study reveals a critical transition temperature at 1000 K beyond which bilayer edge folding dominates over the formation of single atom loops in strengthening the surface of CNFs. This study also underscores the critical roles played by surface bond types, numbers, and distributions on the large failure strength dispersion observed experimentally in CNFs.

© 2013 Elsevier Ltd. All rights reserved.

1. Introduction

Vapor-grown carbon nanofibers (CNFs) [1] are of primary importance as low-density fillers for structural nanocomposites [2] and thermal protection systems [3], as well as catalyst and electrode materials for energy storage devices such as Li-ion batteries [4] and supercapacitors [5]. CNFs made by floating reactant method mostly consist of oblique graphene layers with concentric cone-stacked or cup-stacked structures, and active edges [6]. In recent years, remarkable progress has been made synthetically in controlling the microstructure and morphology of cone-stacked CNFs, such as diameter, length, wall thickness, location and orientation [7,8]. Growth by chemical vapor deposition technique is typically carried out at low-to-intermediate temperatures up to 1273 K [6]. However, the surface characteristics of CNFs are largely dependent upon annealing and oxidation post-treatments

performed at temperatures in excess of 2000 K [9–12]. Therefore, property predictions in cone-stacked CNFs is challenging because surface structure evolution is difficult to measure during the thermal treatment (TT) at high temperature.

Past experimental and theoretical studies have shown that surface structure has only limited influence on elastic deformation in CNFs [13–15]. A recent atomic force microscopy study [15] indicated that, for large wall thicknesses, the elastic modulus of vapor-grown cone-stacked CNFs subjected to bending deformation becomes independent of the wall thickness (~25 GPa), while the measured values of elastic modulus in double-walled vapor-grown CNFs ranged from 6 GPa to 207 GPa. The elasticity of CNFs depends primarily on the cone angle, which varies from narrow angles (~19°) to wide angles (~113°). However, only five possible cone angles exist in CNFs due to the symmetries of graphene [16–19]. As such, it is possible to predict theoretically the tensile modulus for cone-

* Corresponding author at: Mechanical Engineering Program, School of Engineering, The University of Vermont, Burlington, VT 05405, United States. Fax: +1 802 656 3837.

E-mail address: frederic.sansoz@uvm.edu (F. Sansoz).

0008-6223/\$ - see front matter © 2013 Elsevier Ltd. All rights reserved.

<http://dx.doi.org/10.1016/j.carbon.2013.01.027>

stacked CNFs from the elastic properties of graphene and simple geometric considerations [13,14]. On the contrary, the complex surface structure of CNFs results in large strength scattering and statistical dispersion in failure strength of individual fibers subjected to high-temperature heat treatments [11]. Accurate determination of tensile strength and fracture stress in CNFs is hampered by the randomness of size and distribution of surface flaws resulting from surface bonds. Therefore, elucidating the complex relationship between surface structure and strength in CNFs requires deeper insight into the mechanisms and kinetics of surface bond formation in CNFs at high temperature.

CNFs also play a central role in electrochemical processes for catalysis and energy storage applications due to their high electrical conductivity and chemical reactivity. Interestingly, a large amount of open edges on the surface of as-grown CNFs is favorable for the penetration of electrolytes. Open edges have been shown to dramatically improve electrode capacity and reversibility for the insertion and deintercalation of Li ions in batteries [20], as well as for the charge–discharge performance of electrochemical supercapacitors [5]. Also, past experimental reports showed that CNFs can stabilize the growth and dispersion of metallic nanoparticles to augment catalytic activity, by interactions with step-edges on the surface [21,22]. Clearly, surface bonds formed on the fibers during thermal treatment also proves pivotal in modulating the amount of open edges and active sites for these applications.

An important unsettled question exists whether accurate *in situ* measurements of bonding rates can be obtained experimentally in CNFs under relevant thermal conditions. Also, surface bonds in CNFs have been ignored in past atomistic simulation and theoretical studies [13,14,17,23]. Here, molecular dynamics (MD) computer simulations using a bond reactive interatomic potential were used to dynamically model the creation of surface bonds in cone-stacked CNFs at high temperatures, and their physical deformation under tensile loading. We find a substantial increase in elastic strain limit with no change in elastic modulus in nanofibers thermally treated at temperatures up to 2273 K. This phenomenon is due to the greater resistance of surface bonds to crack propagation. The present study shows evidence for two dominant bonding mechanisms and kinetics in CNFs above or below a critical transition temperature of 1000 K. Our findings suggest that both the number of open edges and surface bonds per unit length, and their surface distribution, are important for strengthening in CNFs, and could be optimized by modulating TT temperatures and cone stacking.

2. Computational methods

A cone-stacked CNF with an apex angle of 112.9° was created by classical MD simulations using the adaptive intermolecular reactive empirical bond order (AIREBO) interatomic potential [24] with the software LAMMPS [25]. The potential took into account both short-distance covalent bonds by the REBO potential and long-distance van-der-Waals interactions by the adaptive Lennard-Jones potential. This wide angle was chosen specifically to maximize bond formation on the surface as the equilibrium axial interlayer distance was found to de-

crease with increasing cone angle. First, a carbon cone was made by folding an angular graphene disk with a diameter of 4.5 nm and a disclination angle of 60° . The disclination boundaries were oriented parallel to two zigzag axes of symmetry (Fig. 1a), which resulted in a perfect cone without defects. To perform cone folding (Fig. 1b and c), one edge atom located at position A in Fig. 1a was fixed in each direction while the displacements of other edge atoms were constrained along the orthogonal direction only. Edge atoms at positions B and C in Fig. 1a were displaced toward each other with a constant velocity of 2.5×10^{-4} nm per time step. The time step was 0.5 fs. A Nose–Hoover thermostat was used to maintain a constant temperature of 1 K in the canonical

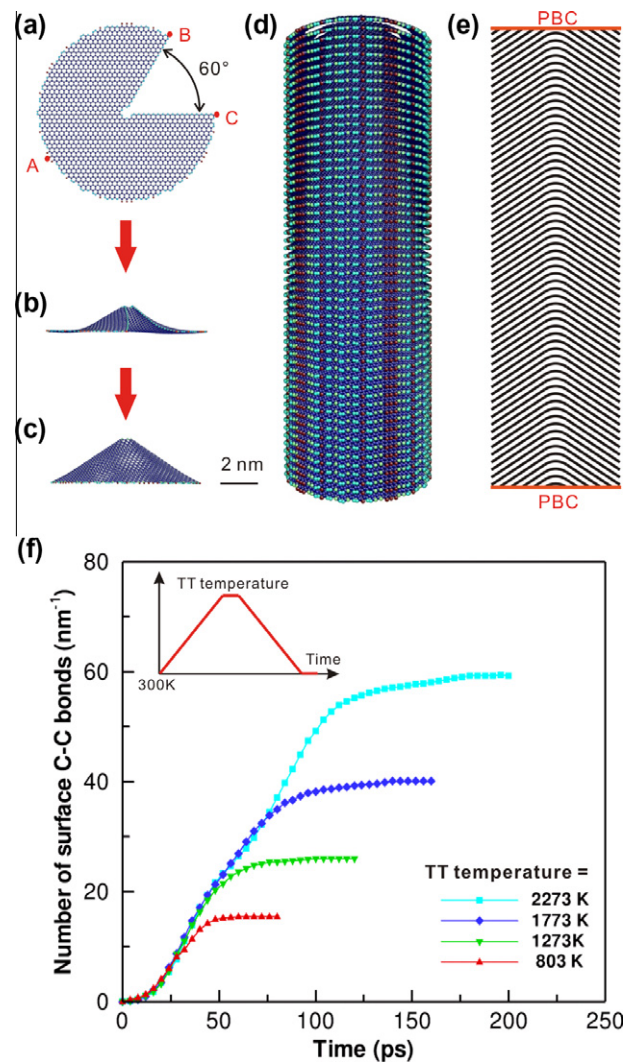


Fig. 1 – Atomistic modeling of a cone-stacked CNF. (a) A circular graphene sheet with an initial 60° disclination is (b) folded from a flat sheet to (c) a seamless nanocone with an apex angle of 112.9° . (d) Fiber structure prior to thermal treatment. (e) Schematic representation showing stacked nanocones with an interlayer distance of 0.34 nm. Periodic boundary conditions (PBC) are applied along the fiber axis. (f) Number of surface carbon–carbon bonds formed during thermal treatment (TT) of a single cone-stacked fiber as a function of simulation time and TT temperature.

ensemble (constant number of particles, volume, and temperature, NVT). A cone was completely formed in 900,000 steps, and further relaxed for another 100,000 steps. Second, a CNF was obtained by stacking 56 cones at an interval distance of 0.34 nm (Fig. 1d and e), the equilibrium distance between flat graphene layers [23]. Furthermore, one internal sp^3 bond was added between each cone in order to take into account the effects of interwall bridging [26]. Interlayer sp^3 bonds were positioned randomly by moving two neighboring atoms on adjacent cones from the equilibrium spacing of 0.34 nm to the sp^3 bond distance of 0.154 nm, while excluding edge atoms. In addition, the spacing between interlayer sp^3 bonds was kept at least four times larger than the sp^2 bond length (0.142 nm). The fiber had periodic boundary conditions applied along its axis, and was free in the other directions, Fig. 1e. The diameter and periodic length were 7.5 and 22.8 nm, respectively, Fig. 1d.

Transformation of the surface structure of the CNF was conducted by TT at temperatures between 400 and 2273 K under zero stress in the isothermal-isobaric ensemble (constant number of particles, pressure and temperature, NPT). A characteristic TT cycle was obtained by heating the molecular system to the TT temperature at a constant rate of 24.5 K ps^{-1} , keeping the system at this temperature for 20,000 time steps, cooling it at the same rate, and equilibrating it for another 20,000 time steps. The time step was 1–2 fs for this process. The number of surface C–C bonds per fiber unit length N was calculated by monitoring the distance between edge atoms of adjacent cones and defining bonding when this distance was less the sp^3 bond length (because sp^3 bond length = 0.154 nm > sp^2 bond length = 0.142 nm > sp bond length = 0.137 nm). Instantaneous bonding rates $\Delta N/\Delta t$ were determined from bond increments obtained every $\Delta t = 4 \text{ ps}$. The maximum instantaneous bonding rate was calculated by fitting the entire rate-vs-time curve by Gaussian functions centered on each peak.

Simulations of fiber deformation in pure tension at 300 K were performed by stretching the simulation box along the periodic length (fiber axis) at a constant engineering strain rate of $1.0 \times 10^8 \text{ s}^{-1}$ using a NVT integration scheme. The time step was 2 fs during deformation. Stress in the loading direction was averaged over the entire volume of the fiber using the Virial theorem. The fiber volume was calculated by parts using 56 cylindrical slices. Snapshots of atomic structures were obtained with Atomeye [27]. Atoms with high to low total energies were colored from red to blue, respectively.

3. Results and discussion

Shown in Fig. 1 is the microstructure of a cone-stacked CNF model prior to TT. The fiber is 7.5 nm in diameter after relaxation at 300 K, and its morphology is very similar to that observed in past experiments [6]. Fig. 1d and e show no surface bond in the CNF model without TT. However, Fig. 1f displays a pronounced increase in the number of surface C–C bonds per unit length when TT temperatures vary from 803 to 2273 K. It is worth noting here that the net increase in surface bonds is more significant in the first half of the TT cycle, up to the middle of the temperature plateau (see in-

set of Fig. 1f). However, as described in detail below, the formation of new surface bonds is associated with different mechanisms and kinetics as a function of time and temperature.

The mechanical behavior of all thermally-treated cone-stacked CNFs deformed in uniaxial tension at 300 K is compared in Fig. 2. The Young's modulus obtained in simulated CNFs is not sensitive to the TT temperatures and is found equal to 20.2 GPa (Fig. 2a), in good agreement with past experimental data [15]. However, the elastic strain limit increases markedly from 4.8% to 9.5% as the TT temperature rises from 803 to 2273 K (Fig. 2b). It can therefore be concluded that nanofibers exposed to high-temperature TT are significantly stronger than those exposed to lower temperatures, although no significant strengthening effect seems to take place below 1000 K. The physical origin for the strengthening is investigated in Fig. 3. Fig. 3a and b show a structural transformation on the surface of fibers thermally treated at high temperature. A large amount of open edge atoms spontaneously formed closed loops between adjacent cones (Fig. 3b). Formation of surface loops at high temperature has been routinely confirmed in experiments [1,4,10–12], and has been proposed as a mechanism to decrease capillary energy [28]. In addition,

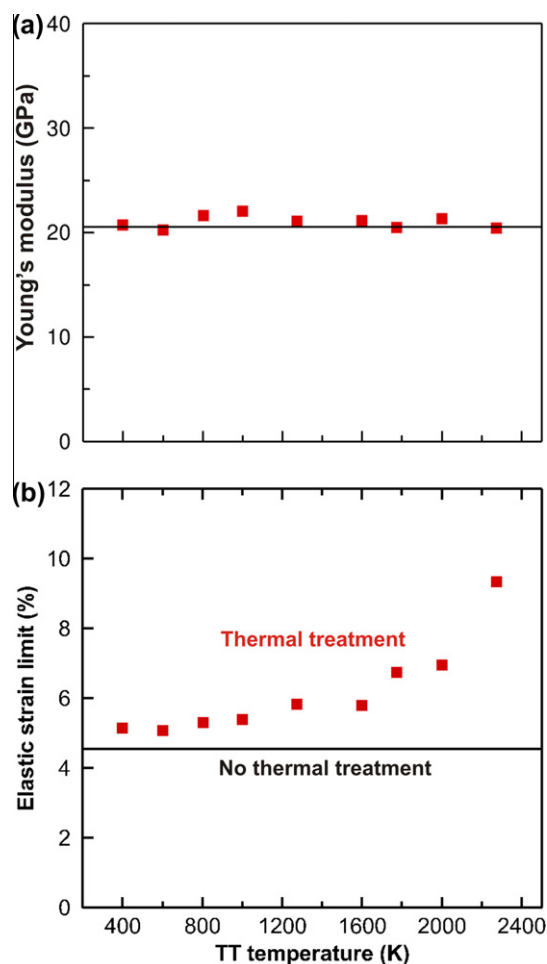


Fig. 2 – Effect of TT temperature on tensile properties of CNFs at 300 K. (a) Young's modulus. (b) Elastic strain limit. Data for fibers without TT are indicated by solid lines.

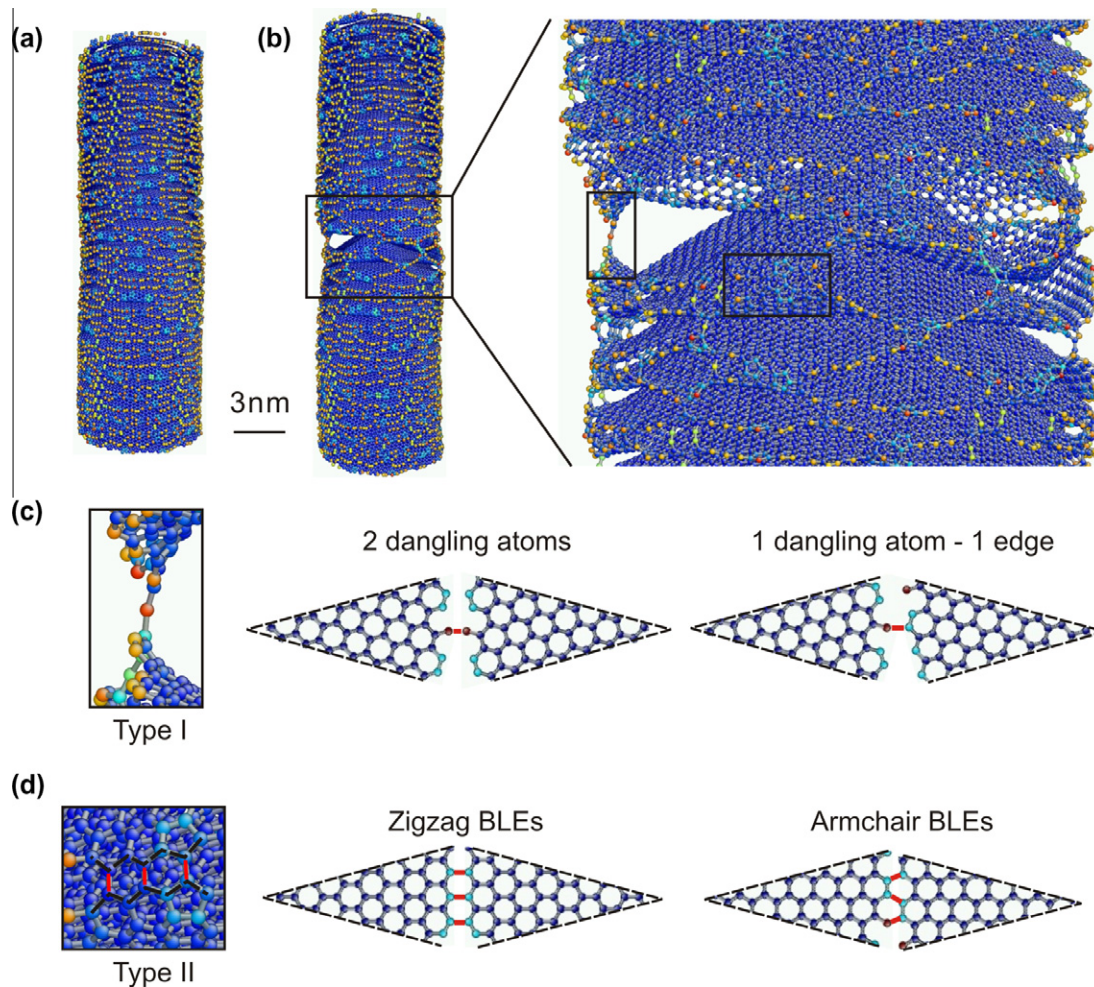


Fig. 3 – Atomic mechanisms of surface bond formed after thermal treatment of a CNF at TT = 2273 K. Microstructure of fiber under (a) zero applied strain and (b) 9% tensile strain. (c) Type-I bonding related to single atom loops from dangling edge atoms. (d) Type-II bonding related to attachment of either zigzag or armchair bilayer edges (BLEs).

Fig. 3b shows that, at the elastic limit, random cracks nucleate at the free surface and propagate inside the fiber between cones by interlayer decohesion and sliding. However, surface loops are found to resist the propagation of surface cracks and, therefore, are the primary carriers of strength in thermally treated CNFs.

Furthermore, a close inspection of the surface evolution of fibers during TT reveals two dominant bonding mechanisms, framed areas in inset of Fig. 3b. On one hand, type-I bonding is associated with the formation of energetically stable loops between either 2 dangling edge atoms with high energy or 1 dangling atom and 1 sp^2 -bonded armchair or zigzag edge atom, Fig. 3c. Single atom loops are accompanied by high-energy topological defects such as pentagons and heptagons needed to compensate for the orientation change and relieve edge stresses. On the other hand, type-II bonding corresponds to the fusion of two zigzag or armchair bilayer edges (BLEs) [29,30], Fig. 3d. Zigzag and armchair BLEs are curved and folded with the same type of edge in adjacent cones, forming a sequence of sp^2 bonds, which is similar to the process of graphitization in experiments with vapor-grown CNFs

[9–11]. Although zigzag and armchair BLEs are strongly favored, zigzag edges can also be attached to armchair edges in neighboring layers to form an interface made of pairs of pentagons and heptagons in spite of disrupting the covalent bonding network [31,32].

Theoretically, the folding curvature of zigzag and armchair BLEs results from a competition between the out-of-plane elastic bending energy and van-der-Waals adhesion energy between two graphene layers. Here, elastic folding is a low-energy process leading to an exceptional stability of zigzag and armchair BLEs. Also, although van-der-Waals adhesion contributes to fiber stiffness and strength, such interaction is expected to be weak in CNFs, as the diameter (d) decreases, because the van-der-Waals contribution scales stronger with the fiber diameter ($\propto d^2$) than the contribution of perimeter bonds (only $\propto d$). In the present study, this hypothesis is confirmed because cones in fibers without TT are found to easily open and slide during deformation, as opposed to the behavior of thermally-treated fibers. Therefore each bonding mechanism likely provides greater fracture resistance to the propagation of surface cracks by impeding sliding between graphene cones.

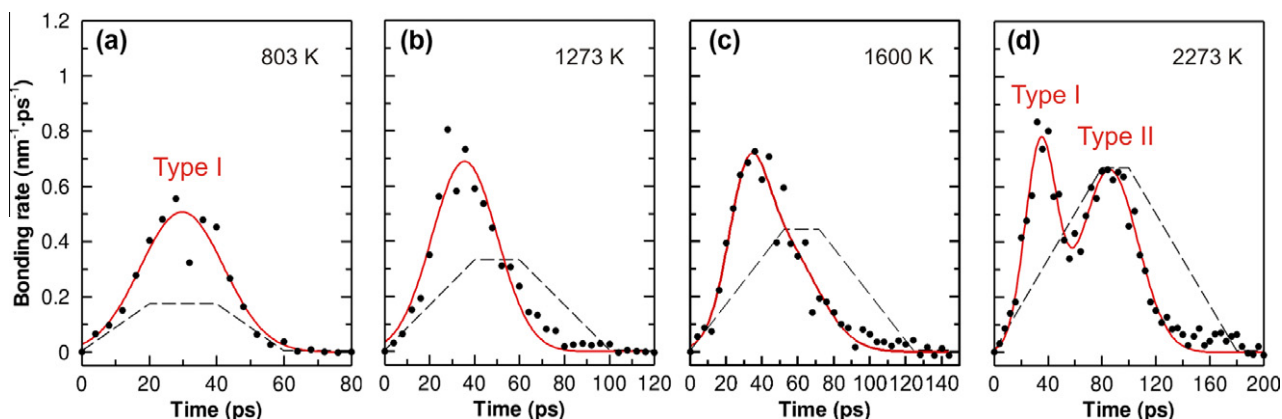


Fig. 4 – Kinetics of bond formation at the surface of a cone-stacked carbon nanofiber with increasing TT temperature. TT cycles are shown in dashed lines. The bonding rates fitted by red curves show two distinct peaks at high temperature related to type-I bonding and type-II bonding, respectively, but only one peak at low temperature.

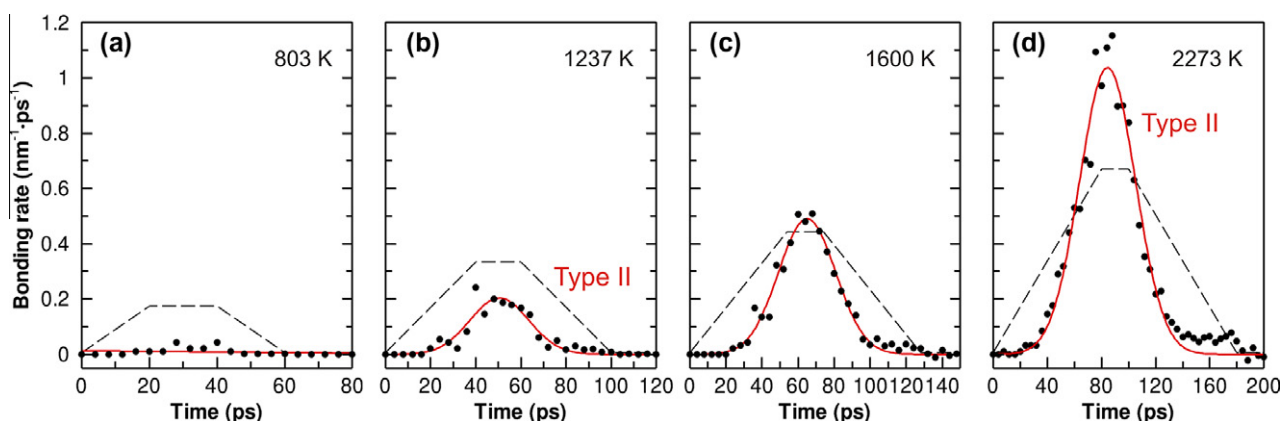


Fig. 5 – Kinetics of bond formation at the surface of a cone-stacked carbon nanofiber without dangling edge atoms. The single peak observed is related to type-II bonding only.

A caveat remains that the atomistic simulation timescales are several orders of magnitude smaller than in experiments, and thus heating rates are significantly higher. Therefore, more meaningful results are obtained in Fig. 4 in terms of surface bond kinetics, in an attempt to differentiate the activation energy of each bonding mechanism. A salient feature in Fig. 4 is that the bonding rates show a single peak at temperatures below 1600 K, and two distinct peaks at 2273 K. By comparing these results to the surface evolution as a function of simulation time, we discover that the first and second peaks result exclusively from either type-I bonding or type-II bonding, respectively. To support this finding, we have also performed a series of TT simulations on CNFs that do not initially contain any dangling atoms; thereby precluding the occurrence of type-I bonding. In this case, the bonding rates show only one peak related to type-II mechanism (Fig. 5), confirming that the second peak in Fig. 4 is due to the same mechanism.

Therefore, this finding allows us to analyze separately the kinetics of each mechanism as a function of TT temperature. Figs. 4 and 5 show that type-I bonding becomes active when

heating temperatures reaches 803 K, but saturates at higher temperatures. In contrast, type-II bonding requires longer activation time, but dominates at higher temperatures. This conclusion is substantiated by comparing the maximum bonding rates for each peak as a function of reciprocal TT temperature. Fig. 6a reveals that the maximum bonding rate of surface loops from dangling edge atoms saturates at an average value of $0.78 \text{ nm}^{-1} \text{ ps}^{-1}$ when $TT = 1000 \text{ K}$, which also corresponds to the start of BLE folding, Fig. 6b. In Fig. 6, the thermal activation energies for type-I bonding and type-II bonding are found to be 14.88 and 30.49 kJ/mol, respectively. This result agrees well with the notion that the energy barrier required to fuse armchair and zigzag BLEs is at least twice that to join a single loop, assuming that a minimum of two loops corresponds to graphitization. Therefore, Fig. 5 points to the conclusion that type-I bonding saturates when type-II bonding becomes significant at a critical transition temperature of 1000 K.

It should be pointed out that graphitization in simulations is not as extensive as in experiments, which may reasonably well be attributed to the difference in TT timescales, albeit

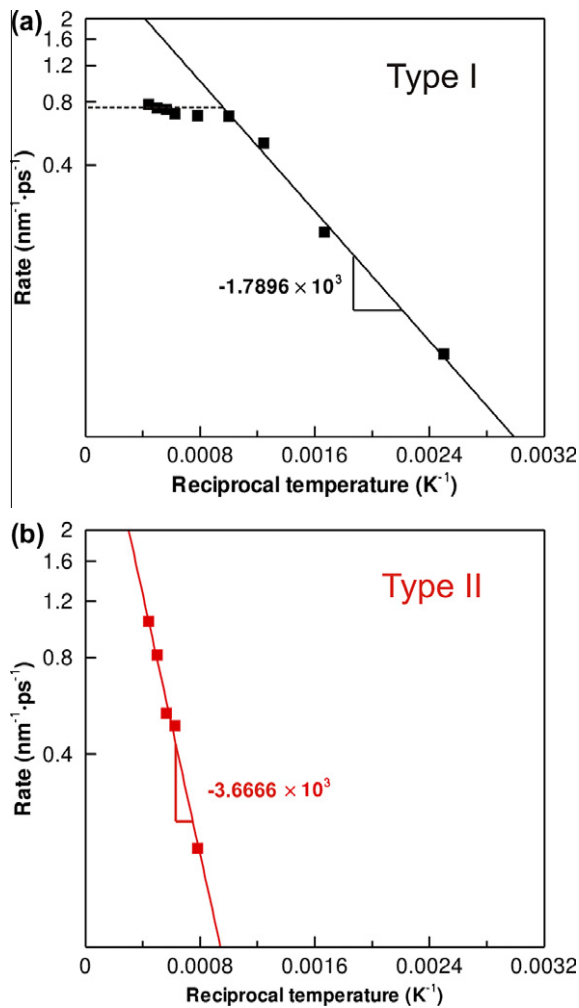


Fig. 6 – Temperature dependence of maximum bonding rate at the surface of a cone-stacked CNF when either (a) type-I bonding or (b) type-II bonding is considered.

more surface bonds created by increasing the annealing time at maximum TT temperature. However, two important implications for the design and properties of microstructures in CNFs can be drawn from the above findings. First, our theoretical study implies that, while the net increase in surface C–C bonds is a continuous process, mechanical strengthening effects due to these bonds only become manifest above 1000 K. Thus BLE folding offers greater resistance to crack propagation under tensile loading than single atom loops. Second, surface strengthening can be raised by increasing bond number and degree of graphitization associated with BLE folding. However, Fig. 7 proves that different bond distributions obtained by altering the initial prescribed velocities in MD simulations, can result in markedly different tensile strengths, despite the same number of initial surface bonds. In experiments, bond distributions could largely be affected by size and random cone stacking, in contrast to the fiber morphology with perfect cone stacking modeled in this study. Therefore, our findings suggest that reducing the statistical dispersion in failure strength of individual CNFs requires additional control over the type, number and distribution of surface bonds.

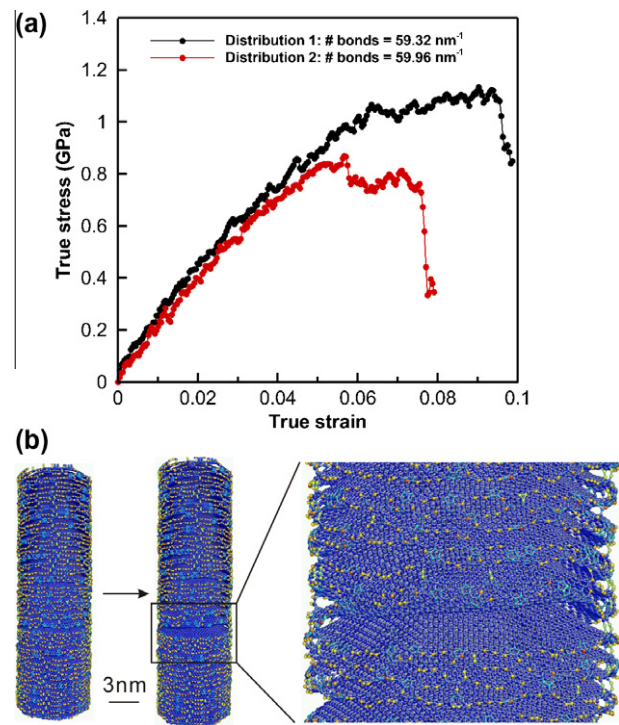


Fig. 7 – Significance of surface bond distribution on strength of thermally treated CNFs with the same number of initial surface bonds. (a) Tensile stress–strain curves at 300 K for fibers thermally treated at 2273 K with different surface bond distributions simulated by changing the initial random velocities. Note that the simulations have been interrupted after the stress drop at yielding. (b) Deformation mechanisms corresponding to the fiber with surface bond distribution 2. In this particular case, the bond distribution is not uniform and results in premature failure by the propagation of a large single crack between two cones. For comparison, the deformation mechanisms corresponding to the fiber with bond distribution 1 are presented in Fig. 3.

4. Conclusions

A detailed theoretical study of mechanisms and kinetics of surface bond transformations on cone-stacked CNFs at high temperatures has been carried out by atomistic computer simulations. A marked improvement in the elastic strain limit from 4.5% to 9.5% was predicted in thermally treated CNFs. This phenomenon is due to newly formed surface bonds providing greater resistance to crack propagation by impeding sliding between graphene cones. Two bonding mechanisms and distinct kinetics associated with either single atom loops from dangling edge atoms or zigzag and armchair BLE folding, have been evidenced. The different kinetics and activation energies reveal a critical transition temperature of 1000 K above which BLE folding dominates over the formation of single atom loops, and more significantly contributes to surface strengthening. This study underscores the critical roles played by surface bond types, numbers, and distributions on the large failure strength dispersion observed experimentally

in cone-stacked CNFs, and the need for additional synthetic control over the initial fiber morphology and TT temperatures.

Acknowledgments

This work was funded by the Vermont Space Grant Consortium/NASA (Vermont EPSCoR) CAN NNX07AT56A, Dr. Michael Wilder, Technical Monitor. The computer resources provided by the Vermont Advanced Computing Center (NASA Grant NNX06AC88G) are also gratefully acknowledged.

Appendix A. Supplementary data

Supplementary data associated with this article can be found, in the online version, at <http://dx.doi.org/10.1016/j.carbon.2013.01.027>.

REFERENCES

- Endo M, Kim YA, Hayashi T, Fukai Y, Oshida K, Terrones M, et al. Structural characterization of cup-stacked-type nanofibers with an entirely hollow core. *Appl Phys Lett* 2002;80(7):1267–9.
- Palmeri MJ, Putz KW, Brinson LC. Sacrificial bonds in stacked-cup carbon nanofibers: biomimetic toughening mechanisms for composite systems. *ACS Nano* 2010;4(7):4256–64.
- Barcena J, Coleto J, Zhang SC, Hilmas GE, Fahrenholtz WG. Processing of carbon nanofiber reinforced ZrB₂ matrix composites for aerospace applications. *Adv Eng Mater* 2010;12(7):623–6.
- Yoon S-H, Park C-W, Yang H, Korai Y, Mochida I, Baker RTK, et al. Novel carbon nanofibers of high graphitization as anodic materials for lithium ion secondary batteries. *Carbon* 2004;42(1):21–32.
- Huang C-W, Wu Y-T, Hu C-C, Li Y-Y. Textural and electrochemical characterization of porous carbon nanofibers as electrodes for supercapacitors. *J Power Sources* 2007;172(1):460–7.
- Terrones H, Hayashi T, Muñoz-Navia M, Terrones M, Kim YA, Grobert N, et al. Graphitic cones in palladium catalysed carbon nanofibres. *Chem Phys Lett* 2001;343(3–4):241–50.
- Takahashi Y, Fujita H, Lin W-H, Li Y-Y, Fujii T, Sakoda A. Synthesis of carbon nanofibers from poly(ethylene glycol) with controlled structure. *Adsorption* 2010;16(1):57–68.
- Melechko AV, Merkulov VI, McKnight TE, Guillorn MA, Klein KL, Lowndes DH, et al. Vertically aligned carbon nanofibers and related structures: controlled synthesis and directed assembly. *J Appl Phys* 2005;97(4):041301–41339.
- Kim YA, Matusita T, Hayashi T, Endo M, Dresselhaus MS. Topological changes of vapor grown carbon fibers during heat treatment. *Carbon* 2001;39(11):1747–52.
- Endo M, Kim YA, Hayashi T, Yanagisawa T, Muramatsu H, Ezaka M, et al. Microstructural changes induced in “stacked cup” carbon nanofibers by heat treatment. *Carbon* 2003;41(10):1941–7.
- Ozkan T, Naraghi M, Chasiotis I. Mechanical properties of vapor grown carbon nanofibers. *Carbon* 2010;48(1):239–44.
- Lawrence J, Berhan L, Nadarajah A. Structural transformation of vapor grown carbon nanofibers studied by HRTEM. *J Nanopart Res* 2008;10(7):1155–67.
- Wei C, Srivastava D. Nanomechanics of carbon nanofibers: structural and elastic properties. *Appl Phys Lett* 2004;85(12):2208–10.
- Uchida T, Anderson D, Minus M, Kumar S. Morphology and modulus of vapor grown carbon nano fibers. *J Mater Sci* 2006;41(18):5851–6.
- Lawrence JG, Berhan LM, Nadarajah A. Elastic properties and morphology of individual carbon nanofibers. *ACS Nano* 2008;2(6):1230–6.
- Eksiöğlu B, Nadarajah A. Structural analysis of conical carbon nanofibers. *Carbon* 2006;44(2):360–73.
- Cheng H-Y, Zhu Y-A, Sui Z-J, Zhou X-G, Chen D. Modeling of fishbone-type carbon nanofibers with cone-helix structures. *Carbon* 2012;50(12):4359–72.
- Krishnan A, Dujardin E, Treacy MMJ, Hugdahl J, Lynam S, Ebbesen TW. Graphitic cones and the nucleation of curved carbon surfaces. *Nature* 1997;388(6641):451–4.
- Smalley RE, Yakobson BI. The future of the fullerenes. *Solid State Commun* 1998;107(11):597–606.
- Zou G, Zhang D, Dong C, Li H, Xiong K, Fei L, et al. Carbon nanofibers: synthesis, characterization, and electrochemical properties. *Carbon* 2006;44(5):828–32.
- La Torre A, Gimenez-Lopez MD, Fay MW, Rance GA, Solomonsz WA, Chamberlain TW, et al. Assembly, growth, and catalytic activity of gold nanoparticles in hollow carbon nanofibers. *ACS Nano* 2012;6(3):2000–7.
- Sebastián D, Calderón JC, González-Expósito JA, Pastor E, Martínez-Huerta MV, Suelves I, et al. Influence of carbon nanofiber properties as electrocatalyst support on the electrochemical performance for PEM fuel cells. *Int J Hydrogen Energy* 2010;35(18):9934–42.
- Zhu YA, Sui ZJ, Zhao TJ, Dai YC, Cheng ZM, Yuan WK. Modeling of fishbone-type carbon nanofibers: a theoretical study. *Carbon* 2005;43(8):1694–9.
- Brenner DW, Shenderova OA, Harrison JA, Stuart SJ, Ni B, Sinnott SB. A second-generation reactive empirical bond order (REBO) potential energy expression for hydrocarbons. *J Phys Condens Matter* 2002;14(4):783–802.
- Plimpton S. Fast parallel algorithms for short-range molecular dynamics. *J Comp Phys* 1995;117:1–19.
- Xia ZH, Guduru PR, Curtin WA. Enhancing mechanical properties of multiwall carbon nanotubes via sp³ interwall bridging. *Phys Rev Lett* 2007;98(24):245501.
- Li J. AtomEye: an efficient atomistic configuration viewer. *Modell Simul Mater Sci Eng* 2003;11:173–7.
- Huang JY, Ding F, Yakobson BI, Lu P, Qi L, Li J. In situ observation of graphene sublimation and multi-layer edge reconstructions. *Proc Natl Acad Sci* 2009;106(25):10103–8.
- Feng J, Qi L, Huang JY, Li J. Geometric and electronic structure of graphene bilayer edges. *Phys Rev B* 2009;80(16):165407.
- Liu Z, Suenaga K, Harris PJF, Iijima S. Open and closed edges of graphene layers. *Phys Rev Lett* 2009;102(1):015501.
- Liu Y, Yakobson BI. Cones, pringles, and grain boundary landscapes in graphene topology. *Nano Lett* 2010;10(6):2178–83.
- Koskinen P, Malola S, Häkkinen H. Evidence for graphene edges beyond zigzag and armchair. *Phys Rev B* 2009;80(7):073401.